Microwave Photonics for Optical Sensors

Javier Hervás, Amelia Lavinia Ricchiuti, Wei Li, Ning Hua Zhu, Carlos R. Fernández-Pousa, *Senior Member, IEEE,* Salvador Sales, *Senior Member, IEEE,* Ming Li* and José Capmany, *Fellow, IEEE*

(Invited Paper)

***Abstract*—This paper presents a review and discussion of the applications of Microwave Photonic techniques and functionalities to the field of optical fiber sensors. A specific end-to end model for its characterization is presented here for the first time that yields the sensitivity of the different figures of merit in terms of measurand variations. Experimental techniques to characterize these systems are presented and applications of two specific microwave photonic functionalities to high-resolution discrete and quasi-distributed optical sensing are illustrated. Future directions of research are also highlighted.**

***Index Terms*—Optical Sensing, Microwave Photonics.**

I. Introduction

Optical fiber sensors have been investigated extensively in the last decades thanks to their intrinsic advantages, such as small size, light weight, immunity to electromagnetic interference, spark free, resistance to chemical corrosion, low insertion loss, high temperature survivability and the ability to make multiple distributed measurements along the fiber length enabled by the nature of the optical fiber [1]. Among the different technologies available for the implementation of optical fiber sensors, fiber Bragg gratings (FBGs) have attracted a considerable attention. FBG fabrication process is quite mature and these devices can be advantageously employed in wavelength-encoded sensing systems that convert the variations of the target measurand into wavelength shifts in the spectral response of the devices. Another added value of FBGs is that they can be easily wavelength multiplexed, which makes them particularly attractive for many applications ranging from structural health monitoring of constructions, automobiles and space vehicles to biomedical monitoring systems. Other multiplexing schemes apart from wavelength-division-multiplexing (WDM) are time-division multiplexing (TDM), optical-frequency-domain-reflectometry (OFDR) and optical-code-division-multiple-access (OCDMA) [2]–[5].

Novel interrogation schemes are based on multiplexing as many FBG sensors as possible [6] - [8] or, alternatively use very long FBG [9] to implement quasi-distributed sensor systems that outperform existing distributed fiber sensing solutions. Fundamentally, a FBG does not isotropically radiate the light as in a spatial scattering process, but rather, it returns it unidirectionally back into the fiber behaving like a partial reflector. This multiplies the efficiency of the process, so the systems employed to interrogate FBG sensors do not require very high pump power to be launched in the sensing fiber, thus avoiding the onset of nonlinear effects and additional noise sources. As a consequence, very simple and cost-effective interrogation systems with comfortable signal-to-noise ratios are employed to interrogate FBG sensors.

Recently, Microwave Photonics (MWP) techniques have been proposed to interrogate multiplexed fiber sensors using [10] – [11]. MWP enables the generation, transmission and processing of radio-frequency (RF) signals with an improved performance as compared to the traditional microwave technologies [12] – [13]. For sensing applications, this technology brings several advantages derived from the fact that it relies on interference in the microwave rather than optical domain. Microwave interferometry is by far more stable and easier to control and, if suitably combined with photonics, provides a remarkable spatial accuracy and interrogation speed [14].

Yet, despite the numerous advantages that MWP brings to the field of optical sensing, its potentials are yet not fully exploited by its research community. In this paper we aim to provide an introduction to the use of MWP concepts for sensing, which can easily and quickly understood by the interested researcher. We then illustrate this paradigm by means of several relevant examples accounting for a variety of recently published contributions in the field.

Manuscript received xxxxxxxx x, 201Y; revised xxxxxxxx x, 201 Y; accepted xxxxxxxxx x, 201 Y. Date of publication xxxxxxxxxx x, 201 Y; date of current version xxxxxxxx x, 201 Y. This work was supported in part by the Spanish MINECO through projects TEC2014-60378-C2-1-R MEMES, and by the Government of Valencia through the Research Excellency Award Program GVA PROMETEO II/2013/012. J. Hervás work is supported by the MECD FPU scholarship (FPU13/04675). Ming Li's work was supported by the National Natural Science Foundation of China under 61377002, 61522509 and 61535012. Ming Li was supported in part by the Thousand Young Talent program. *Corresponding author: Ming Li, ml@semi.ac.cn

J. Hervás, A. L. Ricchiuti, S. Sales and J. Capmany are with the iTEAM Research Institute, Universitat Politècnica de Valencia, Valencia 46022, Spain (e-mail: jaherpe2@teleco.upv.es; amric1@upv.es; ssales@dcom.upv.es; jcapmany@iteam.upv.es).

C. R. Fernández-Pousa is with the Departamento de Ingeniería de Comunicaciones, Universidad Miguel Hernández, Elche 03202, Spain (e-mail: c.pousa@umh.es).

Wei Li, Ning Hua Zhu, Ming Li (contact author), are with State Key Laboratory on Integrated Optoelectronics, Institute of Semiconductors, Chinese Academy of Sciences, Beijing 100083, China (email: liwei05@semi.ac.cn; nhzhu@semi.ac.cn; ml@semi.ac.cn)

The paper is structured as follows. Section II provides a short introduction to MWP systems, their figures of merit and their use in optical sensing configurations. In particular, a general analytical model is derived for sensor systems based on filtered MWP links, which takes into account the effect of all photonic components in the sensor system. This model is presented here for the first time and provides the expressions leading to the computation of the sensitivities of the relevant figures of merit with respect to a given measurand. In section III we address the important topic of the experimental characterization of MWP sensors by means of optical vector analyzers (OVNAs), while Sections IV and V respectively describe the use of two important MWP functionalities, optoelectronic oscillation (OEOs) and filtering for implementing discrete high-resolution optical sensors. MWP based quasi-distributed sensor implementation is discussed in detail in Section VI and finally, the main conclusions an future lines of research are provided in Section VII.

II. Introduction to Microwave Photonics and its Application to Optical Sensing

Microwave photonics (MWP) [12] - [13], a discipline which brings together the worlds of radiofrequency engineering and optoelectronics, has attracted great interest from both the research community and the commercial sector over the past 30 years The added value that this area of research brings stems from the fact that, on the one hand, it enables the realization of key functionalities in microwave systems that either are complex or even not directly possible in the radiofrequency domain and, on the another hand, that it creates new opportunities for information and communication (ICT) systems and networks. In particular, MWP is expected to extend its use in the next years to novel emerging information technology scenarios, such as 5G mobile communications [15]-[16] internet of the things (IoT) [17] and sensing [14].

A. General model for filtered MWP links

The upper part of Figure 1 illustrates the layout and basic operating principles of a generic MWP system. The starting point is an input RF signal with spectrum sidebands centered at frequency $\pm\Omega$, as shown in point 1. This signal which can have its origin either from an RF generator or from the detection by means of a single or an array of antennas modulates the output of an optical source to up-convert its spectrum to the optical region of the spectrum (point 2), such that the sidebands are now centered at $\omega\pm\Omega$ where ω represents the central frequency of the optical source. The combined optical signal is then processed by an optical system composed of several photonic devices and characterized by an overall lumped optical field transfer function $H(\omega)$. The mission of the optical system is to modify the spectral characteristics of the sidebands, so at its output, they are modified according to a specified requirement as illustrated in point 3. Finally, an optical detector is employed to down-convert the processed sidebands again to the RF part of the spectrum by suitable beating with the optical carrier so the recovered RF signal, now processed (as shown in point 4), is ready to be sent to an RF receiver or to be reradiated. The

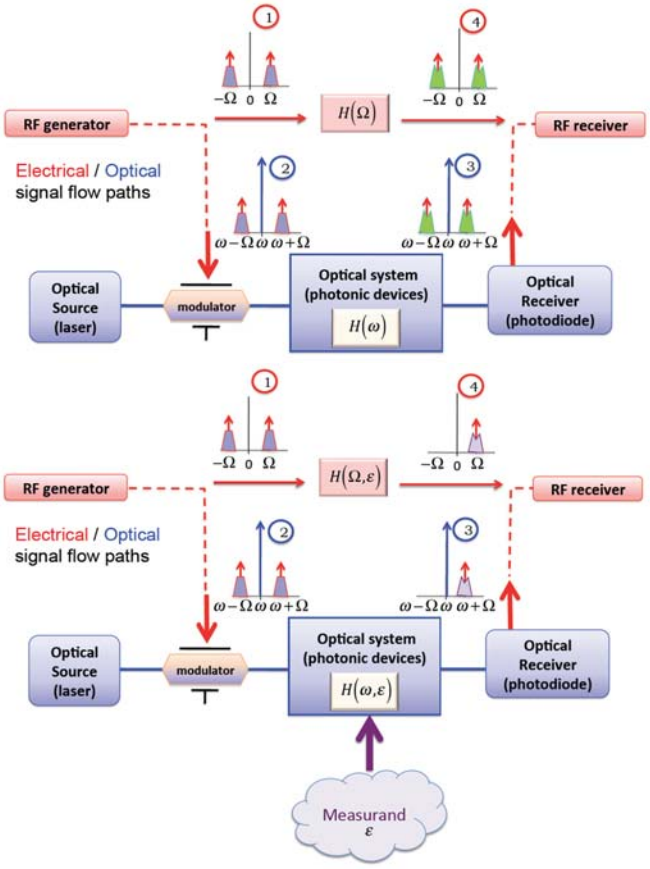

Fig. 1. (Upper) Typical configuration of a MWP link. (Lower) MWP link configuration used as a sensor system to detect a given measurand ε.

overall electrical transfer function $H(\Omega)$ is also shown and must not be confused with the optical field transfer function of the auxiliary optical system.

The performance of these kind of links is commonly evaluated in terms of a set of figures of merit (FOM): the radiofrequency (RF) link gain (G_{RF}), the noise figure (NF) and the spurious free dynamic range (SFDR) [18]. These performance metrics have been computed in [19] for the general system configuration. The radio frequency (RF) Gain of a MWP link is given by [19]:

$$G_{RF}^{I}(\Omega)=\left(\frac{\pi I_{dc}}{V_{\pi}}\right)^{2}\sin(\phi_{dc})\left|\frac{A_{\Omega}^{I}}{2}\right|^{2} \qquad (1)$$

where I_{dc} represents the DC photocurrent, $\phi_{dc}=\pi V_{dc}/V_{\pi}$ the bias phase and A_{Ω}^{I} is a RF signal spectral term defined by $P_s(\omega)$, the spectral density function of the optical source and $H(\omega)$ (see [19] for a detailed description). The noise figure derived in [19] is given by:

$$NF(\Omega)=\left[\frac{4V_{\pi}^{2}}{\pi^{2}Z_{in}k_{B}T}\right]\frac{\left[1-\cos(\phi_{dc})\right]^{2}}{\sin^{2}(\phi_{dc})}RIN_{total}(\Omega)\left|\frac{A_{DC}^{I}}{A_{\Omega}^{I}}\right|^{2} \qquad (2)$$

Where $RIN_{total}(\Omega)$ represents the relative intensity noise due to all noise sources present in the system (see [19] for a detailed description) and A^I_{DC} is the DC signal spectral term [19]. Finally, the dynamic range due to second and third order SFDR are given respectively by:

$$SDFR_2(\Omega)=\sqrt{\frac{2}{RIN_{total}(\Omega)}\frac{\sin^2(\phi_{dc})}{|1-\cos(\phi_{dc})|}\frac{|A^I_{\Omega_1}|^2}{|A^I_{\Omega_1\pm\Omega_2}||A^I_{DC}|}} \quad (3)$$

And:

$$SDFR_3(\Omega)=\left[\frac{2\sin^2(\phi_{dc})}{|1-\cos(\phi_{dc})|RIN_{total}(\Omega)}\right]^{2/3}\frac{|A^I_{\Omega_1}|^2}{|A^I_{2\Omega_1-\Omega_2}|^{2/3}|A^I_{DC}|^{4/3}} \quad (4)$$

Which depend on second and third order intermodulation spectral coefficients $A^I_{\Omega_1\pm\Omega_2}$ and $A^I_{2\Omega_1-\Omega_2}$ (given in [19]).

B. Model for MWP based optical sensors

The MWP link can be employed in sensing applications following the scheme shown in the lower part of Figure 1. Here a measurand ε changes the overall lumped optical field transfer function, which will now depend on it, that is, $H(\omega)\rightarrow H(\omega,\varepsilon)$. Depending on the value of ε the recovered RF signal will change accordingly and variations can be registered in all the three main figures of merit. Assuming that the transfer function depends not only on the frequency but also on the measurand, ε, the spectral coefficients at DC, Ω, $\Omega_1 \pm \Omega_2$ and $2\Omega_1 - \Omega_2$, and the RIN will transform to:

$$\begin{aligned}
&A^I_{DC}\rightarrow A^I_{DC}(\varepsilon)\\
&A^I_{\Omega}\rightarrow A^I_{\Omega}(\varepsilon)\\
&A^I_{\Omega_1\pm\Omega_2}\rightarrow A^I_{\Omega_1\pm\Omega_2}(\varepsilon)\\
&A^I_{2\Omega_1-\Omega_2}\rightarrow A^I_{2\Omega_1-\Omega_2}(\varepsilon)\\
&RIN_{total}(\Omega)\rightarrow RIN_{total}(\Omega,\varepsilon)
\end{aligned} \quad (5)$$

When considering the operation as a sensor we will be fundamentally interested in determining the sensitivity of any of the figures of merit X with respect to the measurand, in other words:

$$S_X=\frac{\partial X}{\partial \varepsilon} \quad (6)$$

Taking (1) and (5) into consideration leads to a relative sensitivity of the RF Link Gain given by:

$$\frac{S_{G^I_{RF}}}{G^I_{RF}}=\frac{S_{A^I_\Omega}}{A^I_\Omega}+\frac{S^*_{A^I_\Omega}}{A^{I*}_\Omega} \quad (7)$$

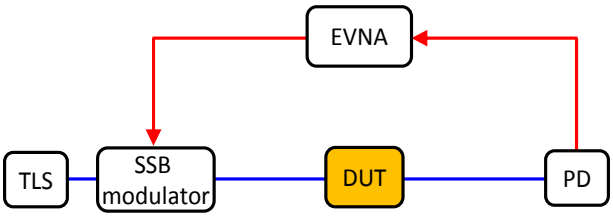

Fig. 2. A typical configuration of OVNA. TLS: tunable laser source, SSB: single-sideband, DUT: device-under-test, PD, photodetector, EVNA: electrical vector network analyzer [21].

Where * denotes the complex conjugate. A similar process can be developed to derive the expressions for the noise figure (NF) and for the spurious free dynamic range (*SFDR*) yielding.

$$\begin{aligned}
&\frac{S_{NF}}{NF}=\frac{S_{RIN_{total}}}{RIN_{total}}+\left(\frac{S_{A^I_{DC}}}{A^I_{DC}}+\frac{S^*_{A^I_{DC}}}{A^{I*}_{DC}}\right)-\frac{S_{G^I_{RF}}}{G^I_{RF}}\\
&\frac{S_{SDFR_2}}{SDFR_2}=\frac{S_{G^I_{RF}}}{G^I_{RF}}-\frac{1}{2}\left(\frac{S_{RIN_{total}}}{RIN_{total}}\right)-\frac{1}{2}\left(\frac{S_{A^I_{DC}}}{A^I_{DC}}+\frac{S^*_{A^I_{DC}}}{A^{I*}_{DC}}+\frac{S_{A^I_{\Omega_1\pm\Omega_2}}}{A^I_{\Omega_1\pm\Omega_2}}+\frac{S^*_{A^I_{\Omega_1\pm\Omega_2}}}{A^{I*}_{\Omega_1\pm\Omega_2}}\right)\\
&\frac{S_{SDFR_3}}{SDFR_3}=\frac{S_{G^I_{RF}}}{G^I_{RF}}-\frac{2}{3}\left(\frac{S_{RIN_{total}}}{RIN_{total}}+\frac{S_{A^I_{DC}}}{A^I_{DC}}+\frac{S^*_{A^I_{DC}}}{A^{I*}_{DC}}\right)-\frac{1}{3}\left(\frac{S_{A^I_{2\Omega_1-\Omega_2}}}{A^I_{2\Omega_1-\Omega_2}}+\frac{S^*_{A^I_{2\Omega_1-\Omega_2}}}{A^{I*}_{2\Omega_1-\Omega_2}}\right)
\end{aligned} \quad (8)$$

Equations (1)-(8) provide a complete framework for the analytic and numerical evaluation of the expected performance of an MWP based optical sensor.

III. RF CHARACTERIZATION OF FBG SENSORS WITH HIGH RESOLUTION USING OPTICAL VECTOR NETWORK ANALYZER

MWP systems in general are experimentally characterized by means of optical vector network analyzers (OVNAs) using the scheme depicted in Figure 2, where the device under test (DUT) represents the optical system. When the DUT is, for example, a FBG-based sensor its resolution is highly dependent on the accurate acquirement of its response. For high sensitive sensors, an extremely narrow bandwidth FBG is essential. FBGs employed in sensing can be ultra-narrowband notch filters [20], which pose a great challenge to demodulation techniques. Optical spectrum analyzers (OSA) usually suffer from low resolution bandwidths (RBW, ~gigahertz or hundreds of megahertz) and are thus not adequate for demodulation. In order to demodulate the FBG sensors with high resolution, OVNAs are required. The resolution of the OVNA can be in the order of kilohertz.

In the configuration shown in Figure 2 the wavelength of a tunable laser source (TLS) is adjusted to a frequency near to that of the central operation spectrum of the DUT. A swept sinusoidal microwave signal from an electrical vector network analyzer (EVNA) is applied to a single-sideband (SSB) modulator. The modulated optical signal consists of an optical carrier and one of the first order sidebands. The first-order sideband sweeps over the magnitude and phase of the DUT.

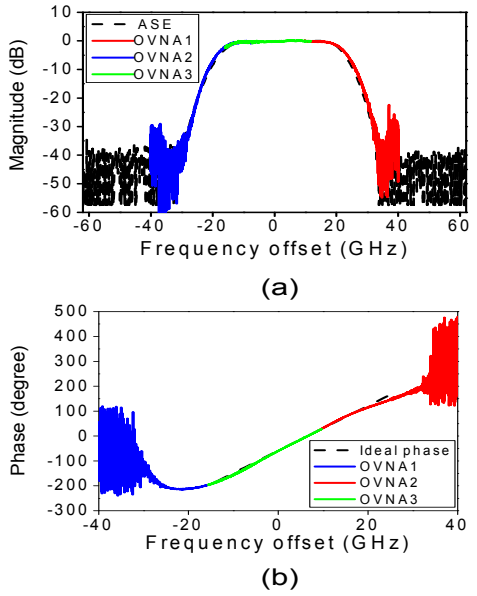

Fig. 3. Measured (a) magnitude and (b) phase response of a DUT with passband response, after [21].

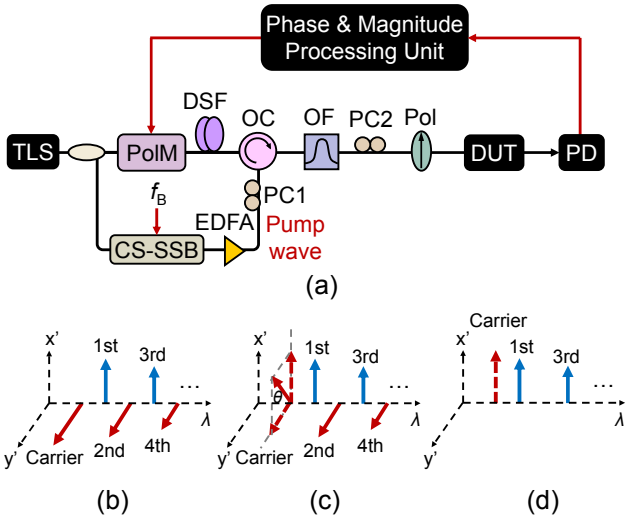

Fig. 4. (a) The SBS-based OVNA with improved accuracy, (b)-(d) the principle behind the proposed scheme. (TLS: tunable laser source, PolM: polarization modulator, DSF: dispersion-shifted fiber, OC: optical circulator, CS-SSB: carrier suppressed single-sideband, EDFA: erbium-doped fiber amplifier, PC: polarization controller, OF: optical filter, Pol: polarizer, DUT: device-under-test, PD: photodetector), after [22].

After detection by a photodetector (PD), the photocurrent is collected by the EVNA. The response of the DUT is therefore obtained by one-to-one mapping between the optical and electrical domains. Normally, the optical carrier stays outside the frequency region under test, so it is significantly suppressed. As a result, the recovered microwave signal in the PD is extremely weak, resulting in large measurement errors.

To overcome this limitation, a SSB-based OVNA has been proposed using segmented measurement in order to keep the optical carrier and sideband located inside the passband of the DUT [21] as shown in Figure 3. First, the response of the DUT at the high frequency side of the optical carrier is obtained. Then the transmission response of the DUT at the low frequency side of the optical carrier is obtained by the second measurement and finally around the central frequencies. In this way, the measurement error or noise generated by the weak optical carrier is eliminated. The transmission response of a flattop bandpass filter has been successfully measured by the proposed OVNA over a frequency range of 80 GHz with a resolution of 25 MHz that it is determined by the EVNA.

An important point to note here is that in order to accurately obtain the response of the FBG-based sensor, measurement errors generated by the nonlinearities of the EOM should be reduced. The errors generally derive from the beating between adjacent optical sidebands. By reducing the modulation index of the EOM, the higher order sidebands can be well suppressed. However, the weak sideband in turn generates measurement errors due to the limited sensitivity of the PD. To circumvent this limitation an OVNA with improved accuracy has been proposed, which is based on polarization modulation and stimulated Brillouin scattering (SBS)-based polarization pulling [22]. The structure and principle is shown in Fig. 4. An optical carrier from a tunable laser source (TLS) is divided into two branches. The upper one is modulated by a polarization modulator (PolM) to generate a polarization modulated signal. The state-of-polarization (SOP) of the even order sideband is orthogonal to that of the odd order one. A dispersion-shifted fiber (DSF) is used as the SBS medium. The lower part generates an optical pump which is a frequency shifted one of the optical carrier. The pump is frequency shifted by a frequency of f_B (SBS frequency shift) using a carrier-suppressed (CS)-SSB modulator. An optical circulator (OC) is added to control the direction of signal and pump lights. An optical filter (OF) is used to realize SSB modulation (see Fig. 4(b)). A polarizer (Pol) is used to remove the even order side-bands including the optical carrier. In this way, the fundamental beating signal between adjacent sidebands does not exist anymore, hence measurement errors are greatly suppressed. However, since the beating between the optical carrier and first order sideband is desired, the SBS-based polarization pulling is used to rotate the SOP of the optical carrier towards that of the odd order sidebands (see Fig. 4(c)). The final result is an optical signal consisting of even-order sideband suppressed components and the optical carrier, as shown in Fig. 4(d). Thus the EVNA mainly collects the contribution from the fundamental tone.

We measured a DUT with notch response to show the feasibility of our method (see Fig. 5). The magnitude response of the DUT is first measured using ASE+OSA. Next, the DUT is also measured using a standard OVNA. The measured result exhibits many errors due to the nonlinearity of the EOM. Finally, the proposed OVNA is used to measure the same DUT. As it can be seen, it agrees well with that obtained using ASE+SOA. The measurement error occurred in the standard configuration is basically eliminated. Moreover, the phase response of the DUT is measured using both the standard OVNA and the proposed one. The phase errors are also reduced

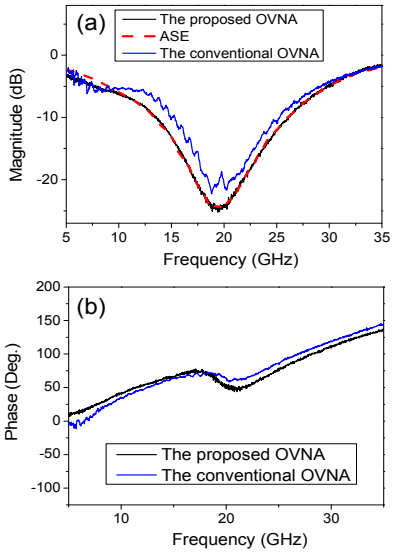

Fig. 5. Measured (a) magnitude and (b) phase responses of the DUT using SBS-based polarization pulling, after [22].

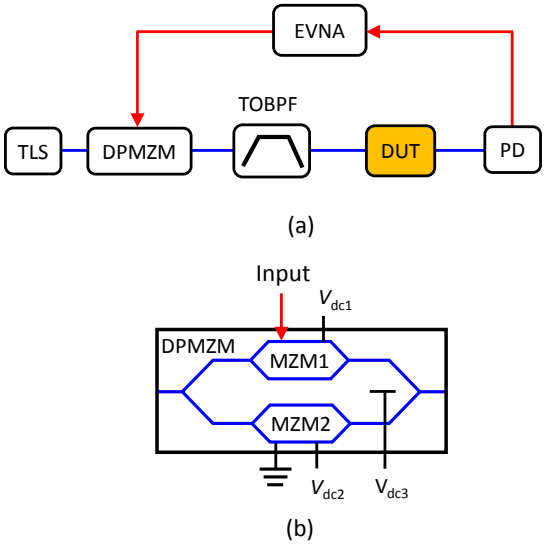

Fig. 6. (a) The schematic diagram of the OVNA based on the DPMZM. TLS: tunable laser source; DPMZM: dual-parallel Mach-Zehnder modulator; TOBPF: tunable optical bandpass filter; DUT: device-under-test; PD: photodetector; EVNA: electrical vector network analyzer. (b) DPMZM configuration, after [23].

using this scheme. The downside of this technique is, however, that it is very sensitive to variations in polarization. To overcome this limitation, we have also proposed a more compact structure to implement an OVNA with improved accuracy. Figure 6 shows the proposed OVNA, which is based on dual-parallel Mach-Zehnder modulator (DPMZM) [23]. The principle of this scheme is very similar to the one based on SBS polarization pulling. The combined use of the TLS, DPMZM, and the TOBPF generates an SSB-modulated signal, which has an optical carrier and odd order sidebands. This modulation format is very promising to reduce the measurement errors generated by the nonlinearity of the EOM. The DPMZM consists of two sub-MZMs. The microwave

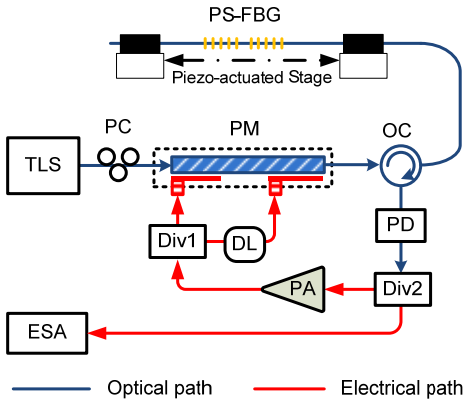

Fig. 7. Schematic of the proposed wavelength interrogation technique of a PS-FBG sensor using an OEO.

signal from the EVNA is driven to the upper MZM1, which is biased at the minimum transmission point to suppress the even order sidebands. The lower MZM2 has no driven signal to let the optical carrier pass through. The output of the DPMZM consists of an optical carrier and odd order sidebands. In addition to removing the measurement errors, the proposed OVNA has larger dynamic range compared with the conventional configuration. In order to verify this property, we carried out an experiment to measure the slope of an optical filter. The dynamic range was improved by around 15 dB. The phase response measured using the proposed OVNA displayed also reduced measurement errors [23].

IV. Femtometer-Resolution Sensor Based on Optoelectronic Oscillator Configuration

Optoelectronic oscillation (OEO) is one of the basic functionalities provided in MWP [24]. An OEO is a mixed photonic-RF cavity designed to provide high quality, low phase noise and stable continuous wave (CW) radio frequency (RF) carriers, but it can also be employed as an enabling block for optical sensing. The schematic of a proposed OEO-based wavelength interrogation system is shown in Fig. 7. The system consists of a TLS, a PC, a two-port phase modulator (PM), a PS-FBG, an OC, a PD, two microwave power dividers (Div1 and Div2), a microwave power amplifier (PA), and a microwave delay line (DL). A lightwave from the TLS is sent to the two-port PM via the PC. The phase-modulated light wave is sent to the PS- FBG through the OC and the reflected signal is sent to the PD. After electrical amplification by the PA, the output of the PD is split into two paths by Div1 and applied to the PM via the two RF ports. A time delay difference between the microwaves signal applied to the two ports is introduced by using a DL in one path. The generated microwave signal at the output of the PD is also sent to an electrical spectrum analyzer (ESA) via Div2. When the PS-FBG is stretched due to the action of a measurand, the resonance wavelength is shifted due to the variation of the grating pitch. As a result, the central (microwave) frequency of the MWP filter is also shifted according to the shifting of the resonance wavelength.

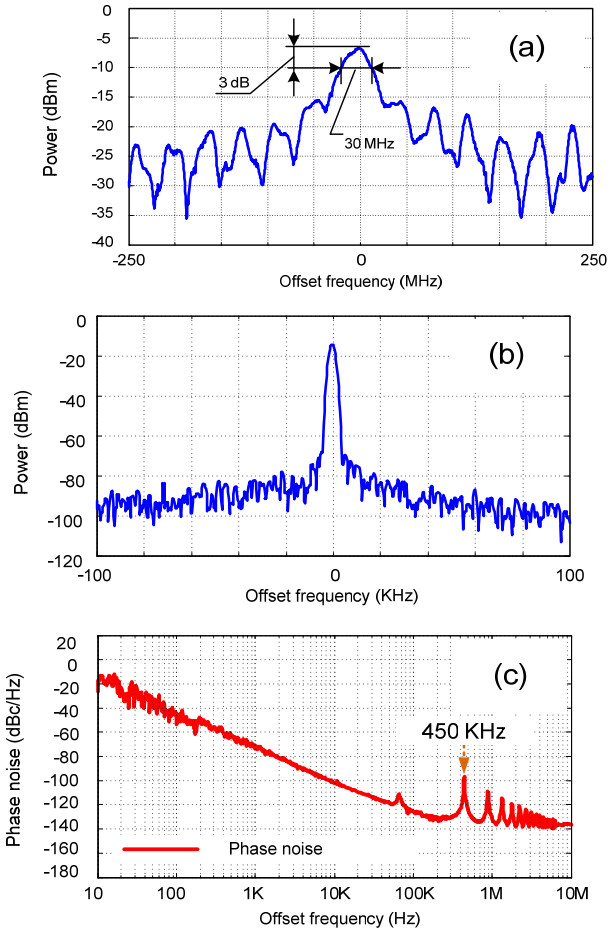

Fig. 8. (a) Measured frequency response of the PS-FBG-based MWP filter vs. offset frequency (around 10 GHz). (b) Spectrum of the 10-GHz microwave signal generated from the OEO loop. (c) Phase noise measurement of the generated 10-GHz microwave signal.

Figure 8 shows the experimental results obtained using this technique in a system where the Bragg wavelength of PS-FBG is around 1549.28 nm, with a full-width at half-maximum (FWHM) width of only about 30 MHz, which mainly determines the bandwidth of the equivalent MWP filter of the open loop OEO, as shown in Fig. 8(a). When the OEO loop is closed, a microwave signal with a frequency of 10 GHz and a 70-dB sidemode suppression ratio is generated as shown in Fig. 8(b). The phase noise performance of the generated 10-GHz microwave signals is given in Fig. 8(c). Several peaks are observed for offset frequencies equal or greater than 450 kHz, corresponding to the longitudinal mode spacing of the OEO. When the resonance wavelength of the PS-FBG is shifted, e.g. due to the target perturbation under test, the frequency of the generated microwave signal is then shifted with a frequency spacing of 450 kHz (i.e., 3.6 fm), and it can be easily measured using an ESA. Figure 9(a) shows the generated microwave signals in the OEO corresponding to different applied strains. The frequency of the generated microwave signal is shifted from about 7 GHz to 17 GHz. Measurements in Fig. 9(b) confirm the expected linear relationship between the applied strain and the frequency of the generated microwave signal.

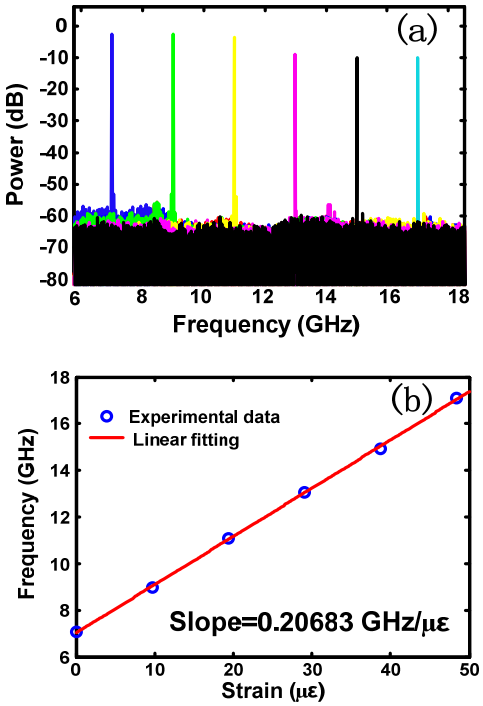

Fig. 9. (a) Spectra of the generated microwave signal for different strains. (b) Relationship between the applied strain and the frequency of the generated microwave signal.

V. Optical Sensors Based on MWP Filtering

The fundamental concept of a sensor system based on a MWP Filter is the exploitation of the impact that the measurand ε has in the overall electrical frequency response, $H(\Omega,\varepsilon)$, as explained in Section II. In the particular case of MWP filtering, the optical system in figure is implemented by means of a discrete-time N-tap MWP filter as depicted in Fig. 10(a). The output of a CW light source is electrooptically modulated with an incoming microwave signal. The output from the electro-optical modulator (EOM) is split into N arms. Each arm has a delay-line and an attenuator (or amplifier) in order to provide a delayed and weighted replica of the original signal. These time-delayed and weighted optical signals are combined together and photodetected.

The combination can be done under a coherent or an incoherent basis. In case of incoherent mixing, the tap combination is insensitive to environmental effects, stable and with a remarkably good repeatable performance. The electrical frequency response $H(\Omega)$ of such a structure is given by:

$$H(\Omega)=\sum_{k=0}^{N-1} a_k e^{-j\Omega\tau_k} \qquad (9)$$

where Ω is the angular frequency, N is the number of reflectors, a_k is the sample weight and τ_k is the sample delay [10]. When $\tau_k = k\cdot\tau$, $\forall k$ Eq. (9) identifies a transfer function with a periodic spectral characteristic; the frequency period is known as free spectral range (FSR) and it is inversely proportional to the spacing, τ, between samples.

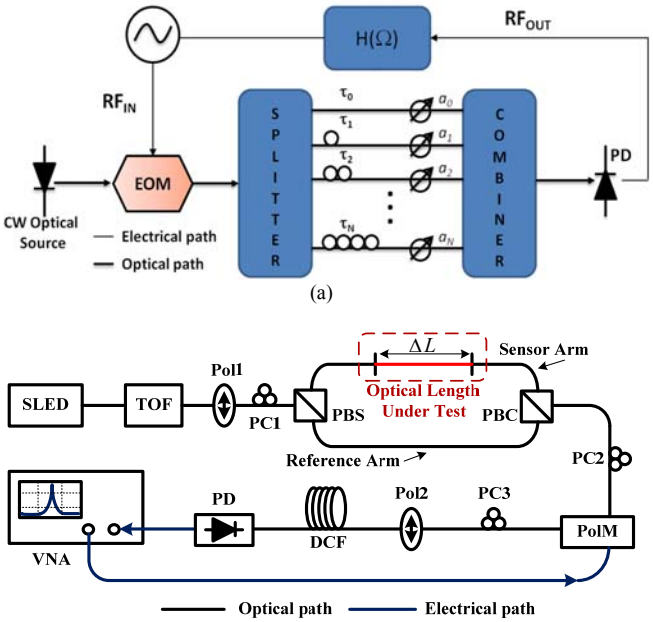

Fig. 10. (a) General scheme of a discrete-time N-tap MWP filter. CW: continuous wave. EOM electro-optical modulator (EOM). PD. photodetetctor (b) Schematic showings of the proposed optical length measurement technique based on a two tap MWP filter. SLED: superluminiscent LED; TOF: tunable optical filter; Pol: polarizer; PC: polarization controller; PBS: polarization beam splitter; PBC: polarization beam combiner; PolM: polarization modulator; DCF: dispersion compensation fiber; VNA: vector network analyzer.

The incoherent regime operation implies that the minimum delay between two consecutive taps, $\tau = \min(\tau_{k+1} - \tau_k)$, has to verify that $\tau_c << \tau$ where τ_c is the optical source coherence time.

We proposed an initial MWP filter to measure optical path lengths with high resolution, as shown in Fig. 10(b). The incoherent light emitted from a superluminiscent LED (SLED) is reshaped by a tunable optical filter (TOF) with a flat-top filtering window and is state of polarization adjusted by means of a polarizer (Pol1). The linearly polarized lightwave is sent to a polarization beam splitter (PBS) via a PC1 and split into two orthogonally polarized lightwaves. The power from the two orthogonally polarized lightwaves is balanced by adjusting the PC1. One of the two orthogonally polarized lightwaves is directed to the optical length under test, which is inserted into the sensor arm, and then combined with the other one at a polarization beam combiner (PBC). The combined orthogonal lightwaves are sent to a PC2 and aligned at ±45° to one principle axis of a polarization modulator (PolM). Since the PolM is a special phase modulator with opposite modulation indices along two principle axes (X and Y axes), the two orthogonal lightwaves (angled at ±45° to the Y axis) will be inversely phase-modulated by the modulation signal, which is generated from an EVNA. The polarization-modulated signal is then sent to a Pol2, which is oriented with the same polarization state of the light in the sensor arm.

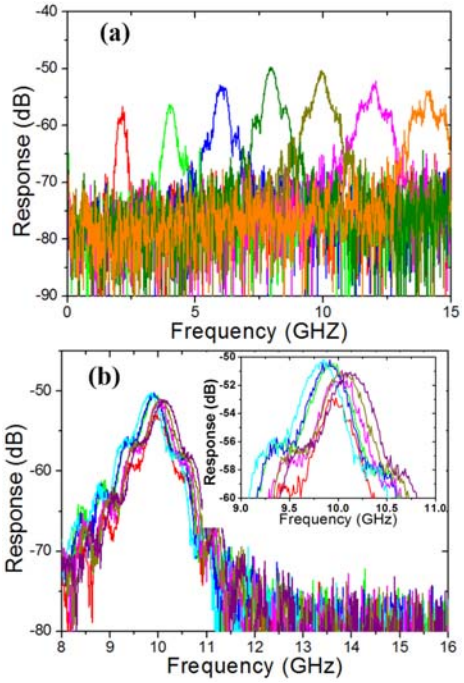

Fig. 11. Measured frequency response of the MPF along with the change of optical length: (a) Center frequency is tuned ranging from 2 to 14 GHz; (b) Center frequency is tuned around 10 GHz, after [25].

Therefore, the optical component with a polarization direction parallel with the transmission axis of the Pol2 will pass through, while the other one with a polarization direction vertical to the transmission axis of the Pol2 will be blocked. Afterwards the output optical signal from the Pol2 propagates through a dispersive compensating fiber (DCF) and is detected by a PD. It can be shown that the MWP filter implemented in this way has a single-bandpass transfer function, where bandpass center frequency can be expressed by [25]:

$$f_c = \Delta t / (2\pi DL) = \Delta L / (2\pi cDL) \quad (10)$$

Eq. (10) shows a linear relationship between the optical length difference and the center frequency of the MWP filter. Therefore, by interrogating the central microwave frequency, the optical length change can be measured. The measurement range is only limited by the bandwidth of the components in the system such as the modulator and the photodetector.

An experiment was conducted where a SLED (Thorlabs s5fc1005s) cascaded with a TOF (Yenista XTA-50) was employed as the incoherent light source. An optical variable delay line (OVDL) was inserted into the sensor arm to emulate the optical length change. A sinusoidal microwave signal from the VNA (Agilent 8720D) applied to the PolM with a frequency sweeping from 50 MHz to 20 GHz, the power of the signal fixed at 10 dBm and a Dispersion Compensation Fiber (DCF) with a value of 425 ps/nm was used to map the modulated optical spectrum into the time domain. The experimental results are shown in Fig. 11(a). By tuning the optical length difference from 0-12 mm between the two arms,

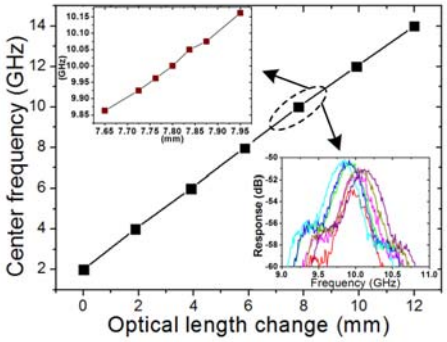

Fig. 12. Relationship between the center frequency of the MWP filter and the optical length change, after [25].

it can be seen that the center frequency shifts from 2 to 14 GHz. Figure 11(b) shows the frequency responses as the center frequency is tuned around 10 GHz and its zoom-in view is shown in the inset. It is worth noting that the 3-dB bandwidth of the passband increases as the center frequency becomes higher. This effect results from the third-order dispersion of the DCF. To overcome this undesirable effect, low third-order dispersion medium such as linear chirped FBGs should be used. It also can be observed that the sidelobe suppression ratio is not identical when the MWP filter moves to higher frequency.

This problem can be fixed by adjusting the PC accordingly. The experimental result shown in Fig. 12 verifies the linear relationship between the center frequency of the MPF and the optical length change. A slope of 1 GHz/mm is obtained which agrees well with the theoretical results. Here, the sensing sensitivity corresponds to the slope with a value of 1 GHz/mm. A zoom-in view for the range from 7.65 to 7.95 mm is presented. In our experiment, a VNA with a frequency resolution of 1 Hz was used and thus a resolution to optical length measurement is estimated theoretically to be 1 pm.

VI. Quasi-Distributed Sensor Systems

Recent works have proposed the use of MWP techniques to implement quasi-distributed sensor systems based on the reflected signal at measurement points [7], [26]-[32]. Initially, we proposed to interrogate a 10cm-long FBG, see Fig. 13 (a). We implemented the sensor system using both a strong FBG (Reflectivity 99%) and a weak FBG (Reflectivity <6%). When the strong FBG is employed, most of the input signal is reflected at the beginning of the FBG [33] – [34]. However, when a local change of the refractive index, due to an event (i.e. temperature variation, induced strain, vibration, etc.), occurs at a certain point along the FBG, a local Bragg wavelength shift will be induced. Then, a second reflected signal is produced at the point where the event is located and a two-tap MWP filter is created [11]. It is possible to determine the location of event by evaluating the FSR of the filter. Figure 13(b) shows the experimental results obtained by moving a hot-spot along the FBG while the inset shows the hot-spot position. As expected, the recovered response is similar to a two-tap MWP filter. The FSR was evaluated with a frequency step of 0.01MHz, which corresponds to an estimated spatial

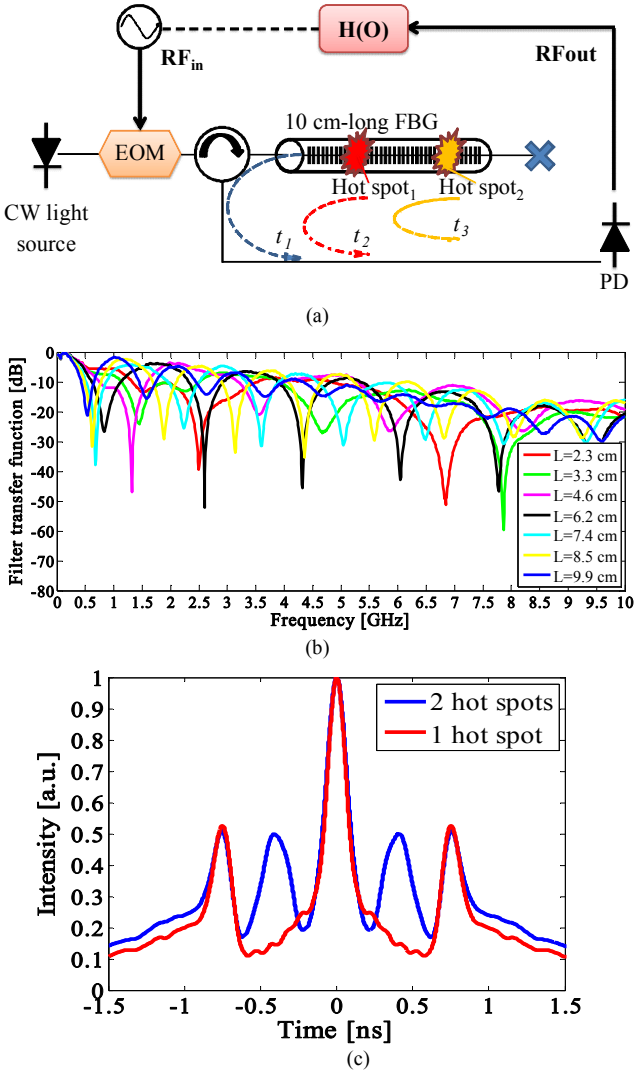

Fig. 13. (a) Illustration of the sensor system based on a 10 cm long FBG. (b) Measured frequency response from the sensor system achieved by moving the hot-spot. Inset, position of the hot-spot, after [11]. (c) Location of hot spots by the IFT of the frequency response of the sensor system, after [11].

accuracy under 0.5 mm. More than one hot-spot can be localized along the FBG. The retrieving of the delays directly from the transfer function is time consuming therefore the most efficient approach to calculate the position of two hot-spots is simply to take the IFT of the transfer function (9). Figure 13(c) shows the IFT of the amplitude of the three tap filter transfer function illustrated in where two hot-spots are placed along the FBG. The minimum distance between hot- spots is limited by the coherence length of the source and the PD bandwidth [11].

Due to the high reflectivity of the sensing FBG, this configuration is not able to detect events having the same magnitude. To overcome this limitation, weak FBG sensors were proposed and employed. The interrogation system is similar to that of Figure 13(a). Some results have been obtained that have validated the use of long weak FBGs to detect more than one event at the same temperature/strain [35].

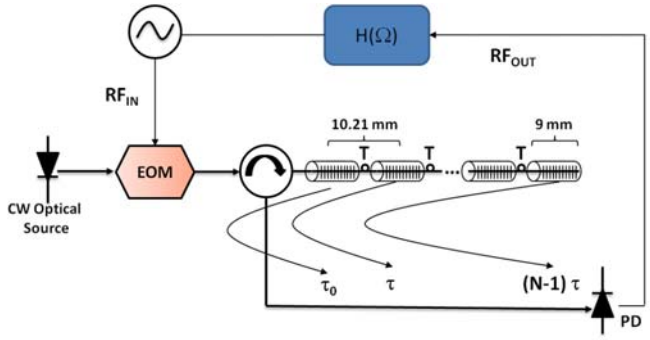

Fig. 14. (a) Schematic view of the 5 m-long distributed sensor based on 500 FBG written in cascade along the fiber.

Nevertheless, for a long-range sensor, ultraweak gratings are required, which ensures low crosstalk level among units in the array and allows the propagation of the optical incident signal over the entire length of the sensor. Since fabricating a long, continuous, and homogenous FBG with no phase hopping and very low reflectivity is an expensive and complicated task [36], we have proposed a sensor made of an array of identical and very weak FBGs written in cascade in coincidence with fiber drawing. We implemented a sensor system composed of an array of 500 equal very weak (Reflectivity ≈ 0.001) FBGs written in cascade in a 5 m-long optical fiber. The nominal length of each FBG is 9 mm and the separation between consecutive FBGs in the array is 10.21 mm, as shown in Fig. 14. The FBG cascade fiber was kindly provided by FBGS International, which fabricates optical fibers by using Draw Tower Gratings (DTGs) Technology [37].

If we assume that the incoming signal is back-reflected with almost the same weight from each of the 500 FBGs the value of the first main resonance (i.e., the FSR span), is related to the distance d between two consecutive FBGs according to:

$$d = \frac{c}{2n_0 FSR} \tag{11}$$

Where c is the speed of light in vacuum and n_0 the effective refractive index. Any filter presents N-1 minima between two consecutive maxima, where N is the number of taps. Hence, the distance between two minima (hereinafter FSR') can be used to calculate the number of taps contributing to the filter response. If an event is produced in the DUT, the effective refractive index will change in a localized area and a new MWP filter will be created. The length of the hot spot (LHS) can be calculated according to the new FSR' of the MWP filter response:

$$d = \frac{c}{2n_0 FSR'} \tag{12}$$

To validate this assumption, an experiment conducted using a frequency span of 500 MHz. The reason for this choice is due to the fact that this frequency range allows a better discrimination of the FSR' on the one hand, and on the other, this moderate span enables the use of devices with modest bandwidth.

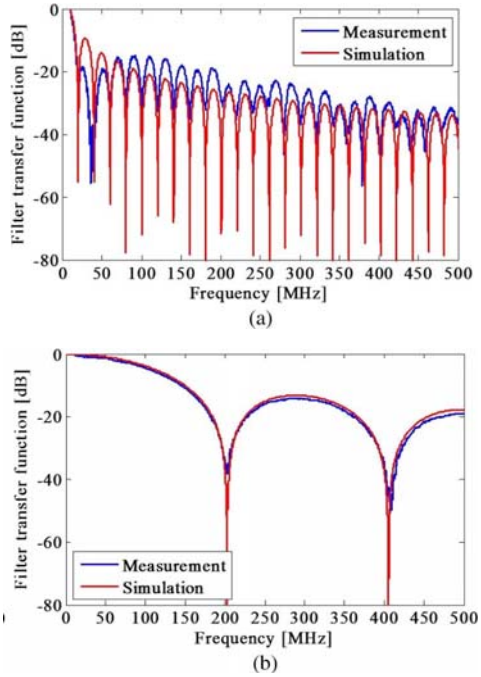

Fig. 15. (a) Frequency response of the MWP filter representing the measured (blue curve) and simulated (red curve) system response. (b) Frequency response of the MWP filter (measured and simulated) obtained by placing a hot spot along the DUT, after [31].

Figure 15(a) (blue curve) shows the transfer function obtained if there are not hot spots along the sensing device, which is in agreement with the theoretical simulation (red curve). The MWP filter presented 500 taps (i.e., 499 minima between one FSR span) and the frequency separation between two consecutive minima is FSR' = 20.23 MHz. When a hot spot is placed, there is a Bragg wavelength shift affecting the FBGs underlying the hot zone [31] and the transfer function of the MWP filter H(Ω,ε) changes. The new distance between minima, FSR', in H(Ω,ε) gives the length of the hot spot. Figure 15(b) shows the new H(Ω,ε). The length of the hot zone is calculated to be 50.72 cm, with a spatial accuracy under 1 mm, dictated by the spatial resolution of the VNA. Furthermore, in order to estimate the position of the spot event, a piece of a single mode fiber (SMF) of length D = 7 m is appended at the end of the DUT and the IFT is taken. In this way, the position of the hot spot (PHS) middle point is measured from the DUT ending, resulting in PHS = 2.8440 m. The minimum detectable hot spot is directly related to the VNA frequency span, Δf_{VNA}, according to:

$$LHS_{\min} = \frac{c}{2n_0 \Delta f_{VNA}} \tag{13}$$

To gain more flexibility, we have proposed the use of a Dispersive Delay Line (DDL), Figure 16, [29]. The FBG peak reflection wavelengths are mapped into radio-frequency (RF) delays by a DDL, allowing the use of standard or weak FBG at the same or different Bragg wavelengths [29], [32].

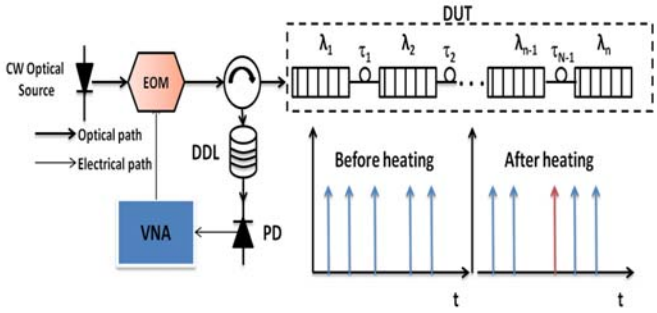

Fig. 16. Illustration of a generic quasi-distributed sensor system interrogated with MWP techniques. DDL. Dispersive Delay Line

The FBG Bragg wavelengths shift under environmental changes, so variations of the delays between the taps of the MWP filter can be determined from the IFT of the system's electrical frequency response. To illustrate the flexibility of the proposed concept further, neither the differences between the Bragg wavelengths of adjacent FBGs in the cascade, nor their shapes, widths, or reflected power, have been fabricated to be uniform. We have implemented a DUT consisted on seven FBGs at different Bragg wavelengths. The widths and shapes of the reflected spectrum are different, as shown in Fig. 17 (a).

Electrical measurements were performed within a bandwidth B = 20 GHz. The DDL were implemented using a single mode fiber (SMF). Due to moderate length (6.83 km) of the SMF, no carrier suppression effects were observed within this frequency span. In any case, carrier suppression amounts to low-pass filtering the electrical response, and thus induced an additional widening of the peaks in the impulse response, but did not change their positions. The proposed method is expected to tolerate situations with moderate carrier suppression, or other low-pass filtering effects such as moderate limitations in modulation or detection bandwidths. A zoom view of the system's electrical frequency response at ~6 GHz is shown in Fig. 17 (b), where the traces show a typical wavy form due to the composition of seven oscillations. Afterwards, the impulse responses were by use of the IFT using a zero-padding technique to smooth the raw traces till one million points. This gives an effective bandwidth B' = 625 GHz or a temporal resolution in the impulse response $\Delta t' = 1.6$ ps. Using a typical value of dispersion D = 17 ps/nm · km, the system's wavelength shift resolution in these experiments is $\delta\lambda_B = 14$ pm.

The impulse response, centered at the peak generated by the heated FBG, is shown in Fig. 17 (c). The time axis does not correspond to the true delays experienced by the microwave signal in the SMF line since it is aliased due to the large frequency step used in the VNA measurements [29]. Since the present method is based on relative time measurements, this fact does not affect its performance. The impulse response peaks correspond to two situations: the blue trace (not heated) has its maximum at 479.202 ns, whereas the maximum of the red trace (heated) is at 479.267 ns. The resolution of the measurement was 8 pm.

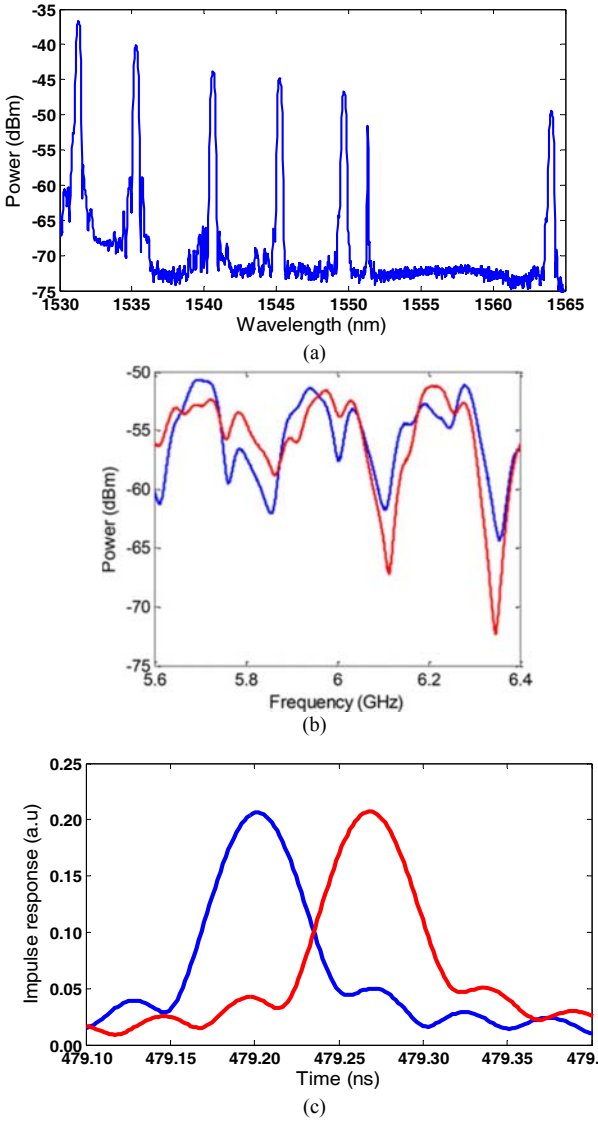

Fig. 17. (a) Reflected spectrum of the seven FBGs employed to implement the DUT. (b) Frequency response of the system when the DUT is under a temperature shift (red trace) and when it is not (blue trace), (c) IFT generated by the FBG at 1540.6 nm at the reference position (blue trace) and when it is heated (red) trace, after [29].

Finally, we have employed the method developed in Section II.B to evaluate the sensitivity of the sensor system configuration of Fig. 16. We consider the case of a six FBG sensor array where the frequency response is depicted in Fig. 18(a), where we also show relative sensitivity of the RF Gain when the measurand acts on the third FBG shifting its wavelength. As it can be observed the most sensitive frequencies are the ones placed around the local minima. Also, we have calculates how the frequency response changes, when the shifted is applied at different FBGs. Fig. 18(b) shows that the minima are shifted depending on the FBG that has been changed. Using the information from Fig. 18(a) and Fig. 18(b) can be inferered, checking only at the most sensitive frequencies, the FBG that has been shifted. Also, we have studied how to improve the sensitivity of the sensor system depending on the configuration. Fig. 19(a) and Fig. 19(b) show

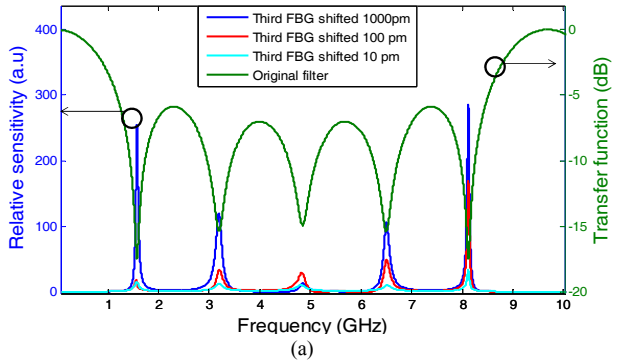

(a)

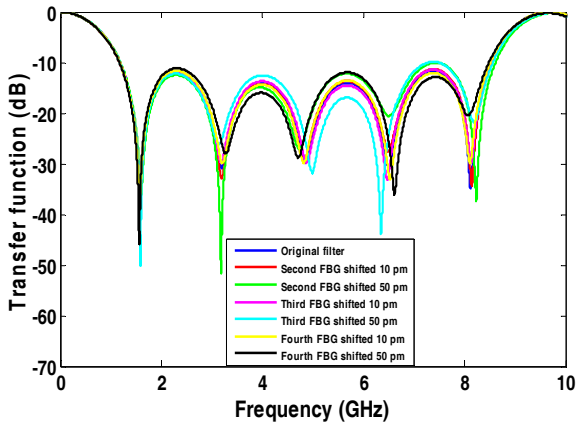

(b)

Fig. 18. (a) Sensitivity of the RF Gain and electrical response of sensor system based on a cascaded of six FBGs. (b) Example of the electrical response of a sensor system for different shifts on the Bragg wavelength of the FBG sensors.

the variation of the frequency response when there is a shift on the third FBG. It can be seen how the sensor system with less distance between consecutive FBGs is more sensitive.

VII. Conclusion

We have reviewed and discussed the use of microwave photonics techniques to the area of optical fiber sensors. The use of MWP techniques brings many advantages inherent to this technology, including electromagnetic immunity, broadband operation, compatibility with optical multiplexing techniques etc.

However, the greatest advantage of applying MWP to optical sensing resides in the fact that optical interference, the effect upon which optical sensors operate, is down-converted to the RF region of the spectrum, leading a much more stable operation regime. Although the main MWP functionalities employed so far for the implementation of optical sensors are based on OEOs and Discrete-time filtering, there is a considerable range for expansion if other functionalities such as instantaneous frequency measurement, photonic RF down and up-conversion, optical beam-forming and arbitrary waveform generation are considered. Future research will, no doubt, address this evolution roadmap.

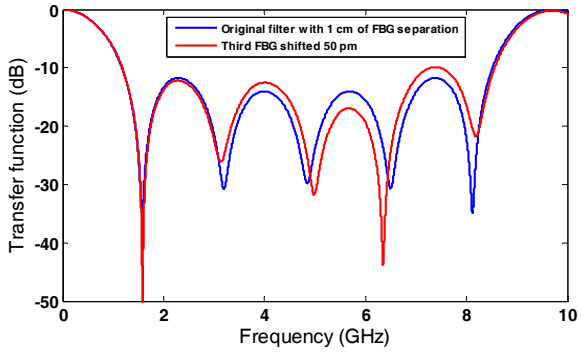

(a)

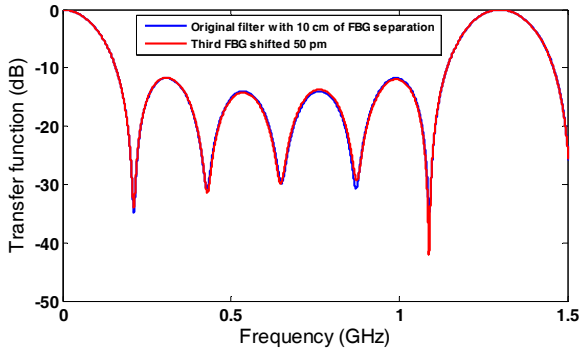

(b)

Fig. 19. Electrical response of sensor system based on a cascaded of six FBGs when the third FBG is shifted (a) the distance between FBGs is 1 cm (b) the distance between FBGs is 10 cm

Acknowledgment

The authors would like to thank Dr. David Barrera from the Universitat Politècnica de Valencia for his valuable help and discussions, and FBGS International for kindly providing the FBG cascade fiber used during the experiment.

References

[1] B. Culshaw, "Optical fiber sensor technologies: opportunities and perhaps pitfalls," *J. Light. Technol.,* vol. 22, pp. 39–50, Jan. 2004.

[2] W. W. Morey, J. R. Dunphy, and G. Meltz, "Multiplexing fiber Bragg grating sensors*,"* in *Proc. SPIE Distributed and Multiplexed Fiber Optic Sensors*, Boston, MA, 1991, pp. 216-224.

[3] D. J. F. Cooper, T. Coroy, and P. W. E. Smith, "Time-division multiplexing of large serial fiber-optic Bragg grating sensor arrays," *Appl. Opt.*, vol. 40, pp. 2643–2554, 2001.

[4] M. Froggatt, B. Childers, J. Moore, and T. Erdogan, "High density strain sensing using optical frequency domain reflectometry," in *Proc. SPIE 4185*, 2000, pp. 249–255.

[5] K. P. Koo, A. B. Tveten, and S. T. Vohra, "Dense wavelength division multiplexing of fiber Bragg grating sensors using CDMA," *Electron. Lett.,* vol. 35, pp. 165–167, Jan. 1999.

[6] C. Hu, H. Wen, and W. Bai, "A novel interrogation system for large scale sensing network with identical ultra-weak fiber Bragg gratings*," J. Light. Technol.*, vol. 32, pp. 1406–1411, 2014.

[7] A. L. Ricchiuti and S. Sales, "Spot event detection along a large-scale sensor based on ultra-weak fiber Bragg gratings using time–frequency analysis," *Appl. Opt.*, vol. 55, pp. 1054-1060, May 2016.

[8] B. A. Childers et al., "Use of 3000 Bragg grating strain sensor distributed on four 8-meter optical fibers during static load tests of a composite structure," in *Proc. SPIE* 4332, 2001, pp. 133–142.

[9] L. Thévenaz, S. Chin, J. Sancho and S. Sales, "Novel technique for distributed fibre sensing based on faint long gratings (FLOGs)," *in Proc.*

SPIE 9157 23rd International Conference on Optical Fibre Sensors, 2014, p. 91576W.
[10] T. Wei, J. Huang, X. Lan, Q. Han, and H. Xiao, "Optical fiber sensor based on a radio-frequency Mach-Zehnder interferometer," *Opt. Lett.*, vol. 37, pp. 647–649, April 2012.
[11] A. L. Ricchiuti, D. Barrera, S. Sales, L. Thevenaz, and J. Capmany, "Long fiber Bragg grating sensor interrogation using discrete-time microwave photonic filtering techniques," *Opt. Exp.*, vol. 21, pp. 28175–28181, Nov. 2013.
[12] J. Capmany and D. Novak, "Microwave photonics combines two worlds," *Nat. Photonics,* vol. 1, pp. 316–330, Jan 2007.
[13] J. Yao, "Microwave photonics," *J. Lightwave Technol*., vol. 27, pp. 314–335, March 2009.
[14] J. Yao, "Microwave photonics for high resolution and high speed interrogation of fiber Bragg grating sensors," *Fiber Integr. Opt.*, vol. 34, no. 4, pp. 230-242, 2015.
[15] J. E. Mitchell, "Integrated wireless backhaul over optical access networks," *J. Lightwave Technol,.* vol. 32, pp. 3373–3382, 2014.
[16] D. Pastor, B. Ortega, J. Capmany, P. Y. Fonjallaz, and M. Popov, "Tunable microwave photonic filter for noise and interference suppression in UMTS base stations," *Electron. Lett.*, vol. 40, pp.997–999, 2004)
[17] A. J. Seeds and K. J. Williams, "Technology focus on microwave photonics," *Nat. Photonics,* vol. 5, pp. 723–736, 2011.
[18] C. H. Cox III, Analog Photonic Links: Theory and Practice, *in Cambridge University Press*, Cambridge, U.K., 2004.
[19] I. Gasulla and J. Capmany, "Analytical model and figures of merit for filtered Microwave photonic links," *Opt. Exp.*, vol. 19, pp. 19758-19774, 2011.
[20] Y. Painchaud, M. Aubé, G. Brochu, and M.-J. Picard, "Ultra-narrowband notch filtering with highly resonant fiber Bragg gratings," *in Bragg Gratings, Photosensitivity, and Poling in Glass Waveguides*, Karlsruhe, Germany, 2010, p. BTuC3.
[21] W. Li, W. T. Wang, L. X. Wang, and N. H. Zhu, "Optical vector network analyzer based on single-sideband modulation and segmental measurement," *IEEE Photon. J*., vol. 6, no. 2, p. 7901108, April 2014.
[22] W. Li, J. G. Liu, and N. H. Zhu, "Optical vector network analyzer with improved accuracy based on polarization modulation and polarization pulling," *Opt. Lett*., vol. 40, no. 8, pp. 1679-1680, 2015.
[23] W. Li, W. H. Sun, W. T. Wang, L. X. Wang, J. G. Liu, and N. H. Zhu, "Reduction of measurement error of optical vector network analyzer based on DPMZM," *IEEE Photon. Technol. Lett*., vol. 26, no. 9, pp. 866-869, May 2014.
[24] L. Maleki, "Recent Progress in Opto-Electronic Oscillator," 2005 *International Topical Meeting on Microwave Photonics*, 2005, pp. 81-84.
[25] Ye Deng, Ming Li, Ningbo Huang, Hui Wang, and Ninghua Zhu, "Optical length-change measurement based on an incoherent single-bandpass microwave photonic filter with high resolution," *Photon. Res.,* vol. 2, no. 4, pp. B35-B39, 2014.
[26] L. Xia, R. Cheng, W. Li, and D. Liu, "Identical FBG-based quasidistributed sensing by monitoring the microwave responses," *IEEE Photon. Technol. Lett.*, vol. 27, no. 3, pp. 323–325, Feb. 2015.
[27] R. Cheng, L. Xia, J. Yan, J. Zhou, Y. Wen, and J. Rohollahnejad, "Radio frequency FBG-based interferometer for remote adaptive strain monitoring," *IEEE Photon. Technol. Lett.*, vol. 27, no. 15, pp. 1577–1580, Aug. 2015.
[28] J. Zhou L. Xia, R. Cheng, J. Yan, Y. Wen, and J. Rohollahnejad, "Radio-frequency unbalanced M-Z interferometer for wavelength interrogation of fiber Bragg grating sensors.", *Opt Lett.*, vol. 15, pp.313-316, Jan 2016.
[29] J. Hervas, C. R. Fernandez-Pousa, D. Barrera, D. Pastor, S. Sales, and J. Capmany, "An interrogation technique of FBG cascade sensors using wavelength to radio-frequency delay mapping," *J. Light. Technol.*, vol. 33, no. 11, pp. 2222–2227, Jun. 2015.
[30] J. Huang, X. Lan, M. Luo, and H. Xiao, "Spatially continuous distributed fiber optic sensing using optical carrier based microwave interferometry," *Opt. Exp*., vol. 22, pp. 18757–18769, 2014.
[31] A. L. Ricchiuti, J. Hervás, D. Barrera, S. Sales and J. Capmany, "Microwave Photonics Filtering Technique for Interrogating a Very-Weak Fiber Bragg Grating Cascade Sensor," *IEEE Photon. Journal*, vol. 6, no. 6, pp. 1-10, Dec. 2014.
[32] J. Clement, G. Torregrosa, J. Hervás, D. Barrera, S. Sales and C. R. Fernández-Pousa, "Interrogation of a Sensor Array of Identical Weak FBGs Using Dispersive Incoherent OFDR," *IEEE Photon. Tech. Letters*, vol. 28, no. 10, pp. 1154-1156, May 2016.
[33] L. R. Chen, S. D. Benjamin, P. W. E. Smith, and J. E. Sipe, "Ultrashort pulse reflection from fiber gratings: a numerical investigation," *J. Light. Tech*., vol. 15, pp. 1503–1512, Aug. 1997.
[34] J. Azaña and M. A. Muriel, "Study of optical pulses-fiber gratings interaction by means of joint time-frequency signal representations*," J. Light. Tech.*, vol. 21, pp. 2931–2941, Nov. 2003.
[35] A. L. Ricchiuti, D. Barrera, S. Sales, L. Thévenaz and J. Capmany, "Long Weak FBG Sensor Interrogation Using Microwave Photonics Filtering Technique," *IEEE Phot. Tech. Letters*, vol. 26, no. 20, pp. 2039-2042, Oct. 2014.
[36] M. Gagné, S. Loranger, J. Lapointe, and R. Kashyap, "Fabrication of high quality, ultra-long fiber Bragg gratings: up to 2 million periods in phase," *Opt. Exp.*, vol. 22, pp 387–398, 2014.
[37] Fbgs-Draw Tower Gratings. [Online]. Available: http://www.fbgs.com/home/
[38] Choi, S.J., Mao, W., Pan, J. K., "Novel RF Interrogation of a Fiber Bragg Grating Sensor Using Bidirectional Modulation of a Mach-Zehnder Electro-Optical Modulator," *Sensors*, vol. 13, pp. 8403-8411, July 2013.